THE JOURNAL OF PHYSICAL CHEMISTRY C

pubs.acs.org/JPCC

Article

Systematic Water Uptake Energetics of Yttrium-Doped Barium Zirconate—A High Resolution Thermochemical Study

Mayra D. Gonçalves, Aleksandra Mielewczyk-Gryń,* Pardha S. Maram, Łukasz Kryścio, Maria Gazda, and Alexandra Navrotsky

Cite This: *J. Phys. Chem. C* 2020, 124, 11308−11316

Read Online

ACCESS | Metrics & More | Article Recommendations

ABSTRACT: A combination of surface area analyzer and microcalorimetry was employed to investigate the in situ water uptake energetics and the mechanism of proton incorporation in yttrium-doped barium zirconate in the temperature range 200−400 °C. The $BaZr_{1-x}Y_xO_3$ solid solutions are made with variable yttrium content (x = 10, 20, and 30 mol %) by a controlled oxidant-peroxo synthesis method. The water uptake increases as the partial pressure of water increases; however, no saturation in the hydration isotherm is observed, implying further reaction at higher p_{H_2O}. The results suggest three distinct regions of hydration energies as a function of water content. The first water uptake enthalpy values showed high exothermicity, −140, −158, and −157 kJ mol^{-1} for $BaZr_{1-x}Y_xO_3$ (x = 10, 20, and 30 mol %), respectively, at 400 °C, and the strong exothermic contribution supports the dissociative incorporation of water. The stepwise in situ hydration energetics is essential to understand the mechanisms of water incorporation and the role of H_2O uptake in transport properties.

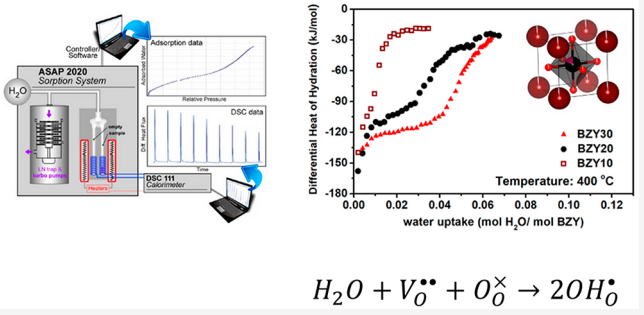

INTRODUCTION

Yttrium-doped barium zirconate (BZY) is the most promising proton conducting electrolyte for solid oxide fuel cells due to its high chemical stability under CO_2-rich atmospheres, mechanical strength, and relatively high proton conductivity at 400−600 °C.[1,2] The $Ba(Zr_{0.8}Y_{0.2})O_{3-s}$ (BZY20) composition was reported to achieve a proton conductivity of 0.1 S/cm at 450 °C.[2,3] Along with optimizing synthetic routes, processing parameters, and morphology, understanding the BZY defect chemistry has also been achieved.[7] The defect chemistry is closely related to the incorporation and mobility of the charge carriers, thus affecting the thermodynamic stability, water uptake, and behavior of proton conductivity as a function of temperature, water fugacity, and electrolyte composition.[7−10] When partially substituting Zr^{4+} ions by the acceptor Y^{3+}, oxygen vacancies are formed for charge balance (1). According to eq 1, every two dopant ions produces one oxygen vacancy. Under a humid atmosphere, the oxygen vacancies allow the incorporation of protons by a dissociative absorption of water. This can be expressed by reaction 2 using Kröger−Vink notation

$$Y_2O_3 + 2Zr_{Zr}^{\times} + O_O^{\times} \rightarrow 2Y'_{Zr} + V_O^{\bullet\bullet} + 2ZrO_2 \quad (1)$$

$$H_2O + V_O^{\bullet\bullet} + O_O^{\times} \rightarrow 2OH_O^{\bullet} \quad (2)$$

where $OH_O^{\bullet}$ is a protonic defect, which diffuses into the bulk simultaneously with the counter diffusion of the oxygen vacancy ($V_O^{\bullet\bullet}$).

Several authors have studied BZY's hydration and defect chemistry by computational simulations and electrochemical and spectroscopic methods.[4,5] On the other hand, only a few research groups have studied the water uptake behavior and calculated hydration enthalpies (ΔH_{hyd}) by recording hydration isobars using thermogravimetric analysis, which is an indirect method for detecting protonic species in solids.[6,7] The reported hydration enthalpies (ΔH_{hyd}) for BZY are in a very broad range (−22 to −93 kJ/mol), and they correspond to the overall hydration enthalpy calculated for the temperature interval at fixed water vapor pressure (usually p_{H_2O} = 0.023 atm). Reproducibility and accuracy among the results are not consistent, since it depends on sample quality, preparation method, and parameters of measurement. Despite high proton conductivity and potential technological application in SOFCs,

Received: February 6, 2020
Revised: April 30, 2020
Published: April 30, 2020

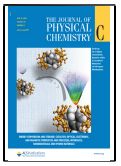

Table 1. Quantitative Chemical Analysis by Electron Microprobe and Surface Area of BZYx, x = 10−30 mol % of Y^{3+}, Solid Solutions Heat-Treated at 1200 °C for 24 h

	stoichiometry by microprobe analysis			
nominal composition	Y	Zr	Ba	surface area (m^2/g)
$Ba_1Zr_{0.9}Y_{0.1}O_{2.95}$	0.095 ± 0.005	0.913 ± 0.005	0.991 ± 0.003	4.48
$Ba_1Zr_{0.8}Y_{0.2}O_{2.90}$	0.208 ± 0.009	0.807 ± 0.006	0.985 ± 0.007	1.69
$Ba_1Zr_{0.7}Y_{0.3}O_{2.85}$	0.294 ± 0.004	0.724 ± 0.005	0.981 ± 0.003	0.43

until now, no systematic evaluation of hydration energetics of BZY solid solutions using *in situ* techniques at variable temperatures has been performed. Isothermal microcalorimetry in combination with a BET surface area analyzer is a promising approach to such determinations, since it allows precise quantification of water uptake and simultaneous *in situ* measurement of heats of reaction upon changing the water vapor pressure.[8−11] Therefore, the goal of this study is a systematic evaluation of hydration enthalpies, which will be useful for investigating the energetics of protonic defect environments and how their stability changes with composition and temperature.[11] This study is the first one to compare heats of hydration obtained using the traditional thermogravimetry method and *in situ* direct isothermal water hydration calorimetry (stepwise hydration of BZY). For the first time, such an experimental approach allowed us to support previous simulation studies.

EXPERIMENTAL PROCEDURES

Yttrium-doped barium zirconate powders with three different compositions hereafter referred to as BZYx (x = 10, 20, and 30 mol % of Y/(Y + Zr)) were synthesized by the oxidant-peroxo method (OPM) inside a glovebox under a nitrogenous atmosphere. The detailed experimental procedure is described elsewhere.[19,20] The precursor powders were placed in alumina crucibles with lids and subjected to heat treatment starting at 800 °C, followed by heating to 1200 °C (10 °C/min) and a dwell time of 24 h, cooling with a rate of 10 °C/min to 800 °C and quenching to room temperature.

The samples were analyzed by powder X-ray diffraction (XRD) using a Bruker AXS D8 Advance diffractometer (Bruker, Madison, WI) operated with Cu Kα radiation. Data were collected in the 2θ range from 10 to 70°, with a step size of 0.02° and collection time of 1 s/step. Phase identification and lattice parameter calculations were performed using Jade 6.1 software (Materials Data Inc., Livermore, CA). The calculated lattice parameters were corrected using the silicon external standard (NIST 640b). Solid-state Fourier-transform infrared (FTIR) spectra of heat-treated samples embedded in KBr were measured using a Bruker Equinox 55 spectrometer, and the instrument was flushed continuously with nitrogen gas. Spectra were collected in the 400−4000 cm^{-1} range with a resolution of 4 cm^{-1}.

Wavelength dispersive spectrometry (WDS) using a Cameca SX-100 electron microprobe (WDS) provided quantitative chemical analysis. The instrument was operated at an accelerating voltage of 15 kV, probe current of 20 nA, and beam size of 1 μm. Sample preparation was performed by pressing the heat-treated powders into 5 mm diameter pellets. Then, they were annealed at 1200 °C/12 h, polished, and carbon coated. The composition of each sample was determined using an average of 10 points. Backscattered electron images and X-ray dot maps were collected to evaluate sample homogeneity.

The surface area of as-synthesized samples was determined by the Brunauer−Emmett− Teller (BET) method using a Micromeritics ASAP 2020 instrument. Prior to the analysis, the samples were degassed under a vacuum at 600 °C for 4 h. Measurements were performed in a liquid nitrogen bath with N_2 as the adsorbent gas. Ten-point adsorption in the range from 0.01 to 0.30 P/P_0 (P_0 = saturation pressure) was collected for each sample. The surface area was calculated using the cross-sectional area of N_2 = 16.2 $Å^2$.

Thermogravimetric analysis of water uptake was performed using a Netzsch Jupiter 449 F1 (Netzsch GmbH, Selb, Germany). Approximately 1.5 g of as-prepared powder was placed in an alumina 5 mL crucible, heated to 1000 °C, and held at this temperature for 0.5 h under dry air to remove water and any surface carbon dioxide. The purge gas (synthetic air) was then saturated with water (p_{H_2O} = 0.021 atm), and the weight change was recorded upon cooling. Data were collected every 100 °C in the temperature range 1000−200 °C with a 3 h stabilization time at each temperature.

In the present study, the hydration experiments were carried out using a well-established combination, Micromeritics ASAP 2020 (Micromeritics Corp, Norcross, GA) and Calvet microcalorimeter (DSC111, Setaram Instruments, Caluire, France). The equipment combination, instrumental design, and measurement procedures were described in detail elsewhere.[10,12−14] The calorimeter instrument was calibrated against the standard enthalpy of fusion of metallic gallium. The water uptake experiments were conducted at three temperatures, 200, 300, and 400 °C. About 0.5 g of sample was hand-pressed into a 5 mm diameter pellet and placed into one side of a forked silica glass sample tube, which fits into the twin calorimeter cells. The empty side of the fork tube acted as a reference. The experiment was comprised of three steps, step 1 - degassing the sample under a vacuum at 600 °C for 4 h, step 2 - cooling to the target temperature followed by the measurement of the free space volume with helium. In the third step, the water uptake experiment was carried out in an incremental dose mode set at 4 μmol of H_2O/dose, allowing 2 h for equilibration between each dose, until the system reached ∼0.023 atm. The procedure was repeated for each temperature. The equilibrium pressure after each vapor increment step and the respective heat effect were simultaneously recorded. The collected data allowed the calculation of the differential hydration enthalpy using eq 3

$$\Delta H_i^{\mathrm{diff}} = \frac{Q_i}{w_i m} \tag{3}$$

where Q_i is the measured heat effect, w_i is the amount of water (in mol/g of the sample), and m is the sample mass.

The same experiment was also carried out on an empty tube to account for water adsorbed on the walls of the forked tube and any manifold leakage. These corrections were necessary because of the low specific surface area of the BZYx powders.

https://dx.doi.org/10.1021/acs.jpcc.0c01049
J. Phys. Chem. C 2020, 124, 11308−11316

RESULTS AND DISCUSSION

Table 1 summarizes the chemical composition and the specific surface area of as-synthesized samples after heat treatment at 1200 °C for 24 h. The surface area of BZYx solid solutions decreases as the Y content increases, ranging from 4.48 to 0.43 m^2/g. The high temperature and extended dwell time of heat treatment promote particle coarsening, which consequently resulted in samples with low surface area.[15] Thus, it may be assumed that the incorporation of water observed in this work mainly occurs within the structure (governed by defect chemistry) rather than on external surfaces, and we, therefore, consider it as bulk water uptake or absorption rather than surface adsorption.

The stoichiometry of the samples determined by electron microprobe is in good agreement with the nominal compositions, Table 1. Barium loss with increasing Y/(Y + Zr) ranges from 0.9 to 1.9% for BZY10 to BZY30. However, the samples still lie in the single-phase region due to the perovskite's capacity to accommodate up to 7% barium deficiency.[6] The results of FTIR (Figure 1) confirm that the barium loss is not related to

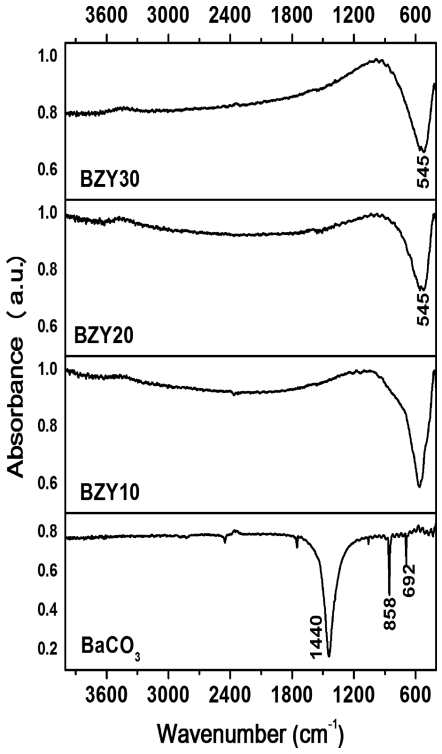

Figure 1. Infrared spectra of heat-treated BZYx samples, with x = 10, 20, and 30 mol %, compared to the $BaCO_3$ spectrum.

the barium carbonate formation. In the infrared spectra, bands typical of the BZY phase are present. The stretching mode for the M−O (M = Zr, Y) bond in BO_6 octahedra was identified as a band centered at ~545 cm^{-1}.[16] This band has an asymmetric shape, especially for BZY10, due to a low-frequency shoulder at 517 cm^{-1} and a broad high-frequency shoulder around 700 cm^{-1}. For both BZY20 and BZY30, the band is split into two peaks at 517 and 562 cm^{-1}, indicating lattice distortions. One small band around 3450 cm^{-1}, related to the O−H stretching mode,[16] was identified for all samples, indicating the initial hydration of as-prepared specimens.

The single-phase nature of the samples was further confirmed by the XRD patterns in Figure 2a, which shows that the reflections are indexed within the cubic perovskite phase (PDF no. 06-0399, a = 4.1973 Å). Figure 2b represents the PXRD pattern of BZYx solid solutions after water uptake measurements. The water uptake did not induce any secondary phase nor diffraction peak broadening. To study more subtle structural changes caused by the formation of protonic defects and hydration, unit cell parameters and the Goldschmidt tolerance factor ($t = \frac{r_A + r_O}{\sqrt{2}(r_B + r_O)}$) were analyzed. The tolerance factor and lattice parameters of each BZYx sample before and after the water uptake experiments were calculated from its respective PXRD patterns (Figure 3).

The lattice parameter increases with increasing yttrium content due to the larger ionic radius of Y^{3+} than that of Zr^{4+}. The water absorption measurements did not induce significant changes in the lattice parameter, which is in line with previous data for acceptor-doped $BaZrO_3$-based materials.[17−20]

Figures 4 and 5 represent the water uptake studies and data collected via the thermogravimetric method. The sample weight changes with temperature under dry and wet atmosphere are presented in Figure 4. The shape of the hydration curves is similar to those reported by Yamazaki et al.[21] In their work, glycine nitrate combustion synthesis was performed, resulting in a micrograin powder with a similar surface area to ours.[6] Therefore, the possible difference between water uptake values should not be attributed to a particular grain size. Figure 5 depicts the total mass gain and proton concentration of investigated samples, showing the change with increasing yttrium content. This result is in agreement with previous findings showing the rise of total proton concentration with the dopant concentration.[21,22] For the lower temperature range (below 500 °C), the uncertainty of the mass determination is higher. The same is also noticed in the case of BZY30 (Figure 4b). A similar effect has been observed by Yamazaki et al.[6] which has been attributed to longer equilibration times at these temperatures Therefore, in this study, the thermodynamic parameters have been calculated only for the region where equilibrium has been reached.

As reported previously, the highest water uptake for the BZY system occurs for the 400−450 °C range in which the hydration reaction is preferred over the dehydration reaction.[23] If one sums the total water uptake at 200−400 °C for each composition (Table 3), the total fraction of sites that are filled is 0.046, 0.176, and 0.239 mol of H_2O/mol of BZYx, respectively, for x = 10, 20, and 30% of Y. That means BZY20 had 88% of the nominally vacant sites available for water uptake, while, for BZY10 and BZY30, 46 and 80% of vacancies could be occupied, respectively. The best performance for BZY systems as a solid electrolyte was shown by the BZY20 composition at 450 °C (1×10^{-2} S cm^{-1}).[24] At 500 °C, the dehydration reaction starts to compete with the adsorption, and at 600 °C, hole conductivity was also reported.[25] Therefore, the proton uptake in our studies has been recorded after an equilibration time long enough to reach a steady state.

Previous impedance spectroscopy and calorimetric studies on BZYx were performed on samples prepared by the OPM synthesis method in a controlled N_2 atmosphere. The results showed that the conductivity is maximum when lower density and cleaner grain boundaries are present in the microstructure; the dopant is still in a dilute regime in the BZ matrix, which occurs for Y concentrations up to 20%, and the temperature of

https://dx.doi.org/10.1021/acs.jpcc.0c01049
J. Phys. Chem. C 2020, 124, 11308−11316

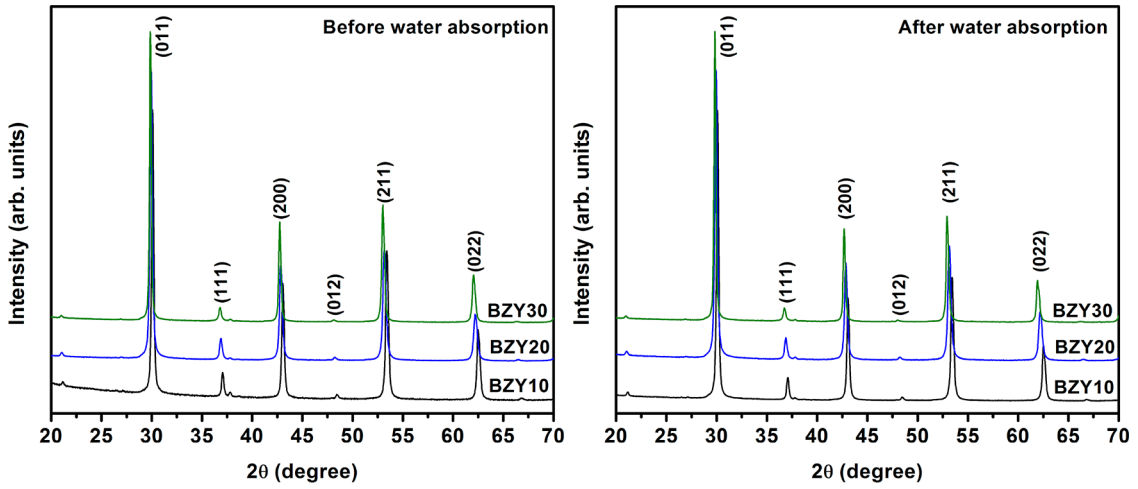

Figure 2. Powder X-ray diffraction patterns of BZYx heat-treated samples, x = 10, 20, and 30 mol % of Y^{3+}, before (a) and after (b) the water uptake calorimetry measurements (Reference PDF No. 06-0399).

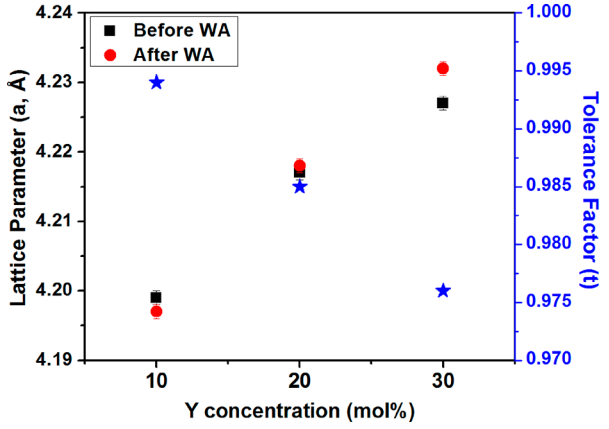

Figure 3. Lattice parameter before and after water uptake measurements and tolerance factor of BZYx, x = 10, 20, and 30 mol %.

the measurement is high enough to allow enhanced mobility of the charge carriers.[22,26] In the present work, despite the higher water uptake at a lower temperature, protons will preferably occupy trapping sites, which makes them mostly unavailable for the conduction process.[21,22]

Figure 5 shows the Arrhenius plot of the equilibrium constant (4) of the reaction of proton incorporation (2).

$$K_w = \frac{[OH_O^\bullet]^2}{p_{H_2O}[V_O^{\bullet\bullet}][O_O^\times]} \quad (4)$$

The calculated values are based on the nominal dopant concentration and assuming that the hole concentration under the measurement condition is negligible. Therefore, the equilibrium constant can be estimated by using the below equation (5).[6]

$$K_w^{p=0} = \frac{4[OH_O^\bullet]^2}{p_{H_2O}(6 - [Y'_{Zr}] - [OH_O^\bullet])([Y'_{Zr}] - [OH_O^\bullet])} \quad (5)$$

$$K_w^{p=0} = \exp\left(\frac{\Delta S_w}{R}\right)\exp\left(-\frac{\Delta H_w}{RT}\right) \quad (6)$$

Based on eq 6, the parameters of the energetics of hydration have been calculated; see Table 2. These values are in reasonably good agreement with prior data.[2,3,6] The small differences could be consequences of several experimental parameters, especially differences in barium stoichiometry, which are known to affect the oxygen vacancy availability.[22]

The values of enthalpy of hydration for all examined compositions at a lower temperature (100−500 °C) are equal within the uncertainty range. At higher temperatures, a difference in hydration enthalpy for two temperature regions is observed, which reflects the differences between competitive reaction rates between proton dissolution within the structure and dehydration. Takahashi et al. have shown, in a DFT study, that the crucial factors influencing proton concentration are the stability of oxygen vacancies and the availability of a stable protonic site with structural distortions during hydration. They reported that the degree of Y-doped BZO hydration is increased and more exothermic when the associated defects are isolated, meaning when they do not interact with each other.[27] Therefore, one should assume the vacancy concentration will influence the energetics of hydration and, consequently, the conductivity. In our study, the concentration of oxygen vacancies, resulting from doping, does not differ much from the values reported by other authors. Therefore, it is reasonable to assume similar energetics of hydration. The differences between the values obtained can be a result of varying sample morphologies and resulting in different saturation times.

Putilov and Tsidilkovski[28] showed that the trapping of protons is reflected in more exothermic enthalpies of hydration and causes a decrease in the hydration entropy. In contrast, trapped oxygen vacancies lead to less favorable hydration energetics. Simultaneously, the filling of oxygen vacancies upon hydration decreases the system entropy, which is related to a more ordered defect distribution. Therefore, the resulting behavior of the hydration thermodynamic functions is determined by the trapping of both protons and vacancies. These facts explain the more exothermic enthalpy of formation at a higher temperature for BZY30. Moreover, it is also consistent with our previous thermodynamic studies, which show that defect clustering should favor proton trapping, for yttrium contents higher than 20 mol %.[22]

Figure 6 shows the total amount of H_2O absorbed (θ, in moles) per mole of BZYx as a function of water partial pressure.

https://dx.doi.org/10.1021/acs.jpcc.0c01049
J. Phys. Chem. C 2020, 124, 11308−11316

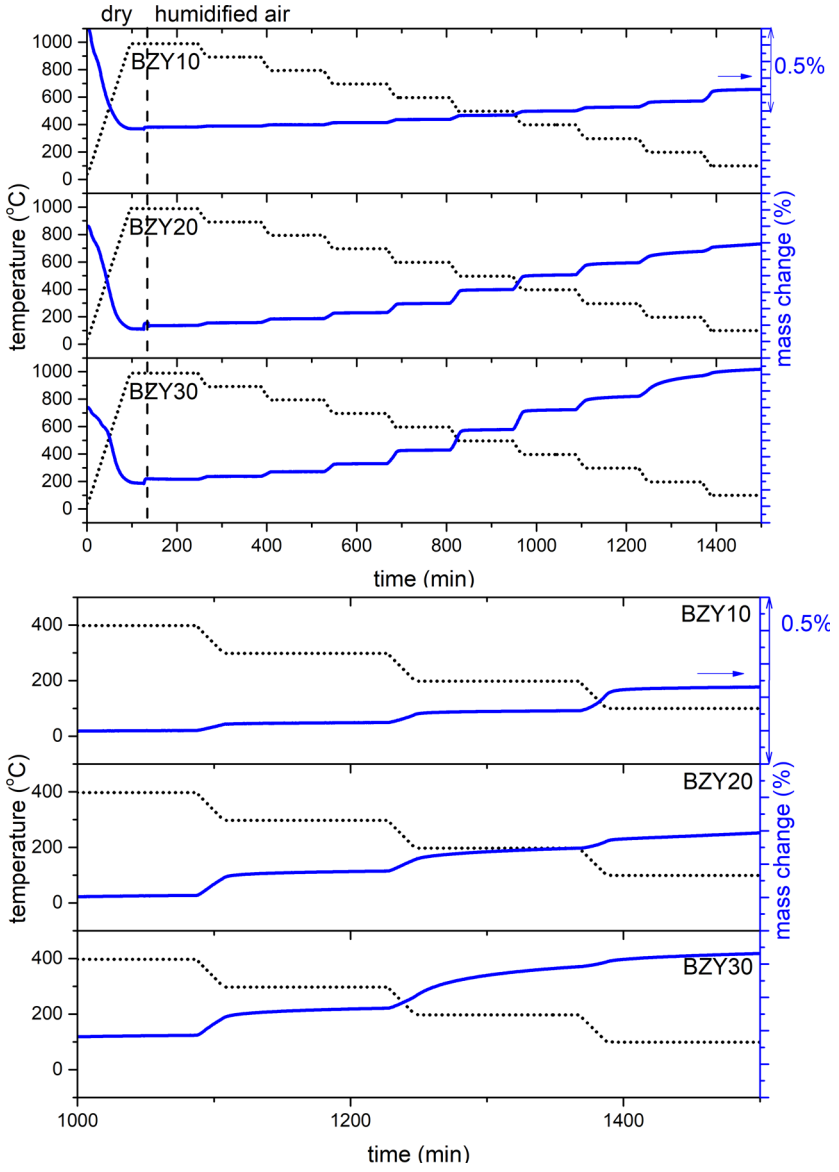

Figure 4. (a) Weight change of BZY10, BZY20, and BZY30 samples and temperature as a function of time under a water partial pressure of 0.019 atm. (b) Zoomed in results showing saturation for lower temperature regions.

The shape and trends of water vapor uptake isotherms are similar for all of the compositions and are related to the hydration mechanism. In the temperature range studied, the presence of electron holes may be neglected and the observed behavior upon hydration can be attributed solely to proton defect incorporation into structure.[6]

Figure 7 and Table 3 present the differential enthalpies of water incorporation into barium zirconate structure at 200, 300, and 400 °C. Hydration enthalpies for all measured samples are independent of the dopant concentration for both thermogravimetric and direct calorimetric measurements, probably due to the similarity in ionic radii and valence electron configuration between dopant Y and host Zr. However, direct calorimetric measurements show three distinct regions in Figure 7. The region corresponding to the lowest proton concentration can be attributed to surface reactions/exchange, while the middle region is probably linked to bulk water incorporation. First, protons incorporate into the sites with the highest affinity, and when these sites are full, the hydration will proceed toward the less favorable sites. At the highest water uptake, this process starts to be limited by proton diffusivity through the bulk. Polfus et al. have shown that the space-charge layer forming within the BZY sample affects the defect concentration near the surface, changing the affinity for species adsorption, including dissociative adsorption.[30] According to them, dissociative water incorporation in barium zirconate is more favorable than molecular adsorption. This is supported by the strongly negative enthalpies of hydration at low coverage. The saturation of the surface, according to their calculations, leads to a rather significant distortion of the surface. Such rearrangement explains the rapid change in the slope of the hydration enthalpy curve for a certain value of incorporated protonic defects.[5] The water uptake is strongly dependent on the surface termination, and this depends on both the synthesis method and the thermal treatment. The dopant can either segregate on the surface or be fixed in a so-called frozen-in situation, resulting from slow diffusivity. Defect segregation along with space-charge can significantly affect the surface chemistry of BZY influencing its hydration. According to Kim et al.,[31] positively charged proton and oxygen vacancy segregation at the surface forms a high

https://dx.doi.org/10.1021/acs.jpcc.0c01049
J. Phys. Chem. C 2020, 124, 11308−11316

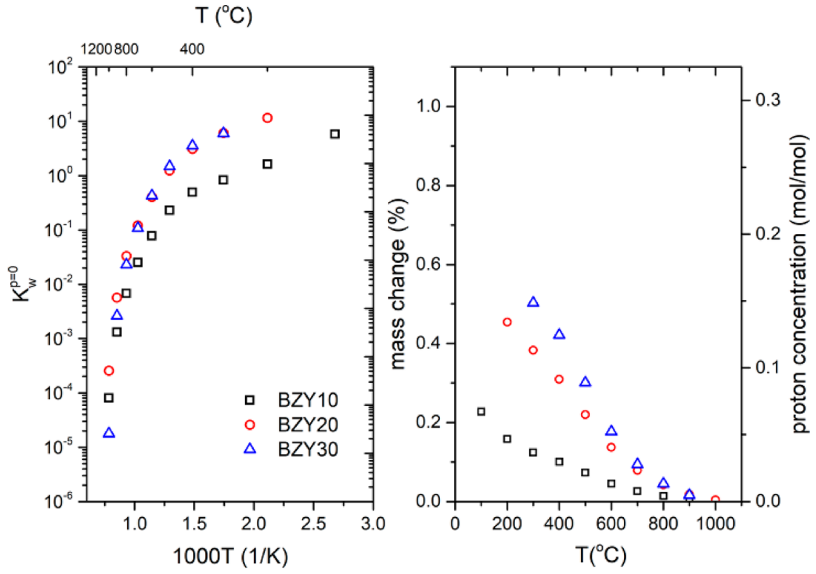

Figure 5. (a) Equilibrium constant for water incorporation reaction in the BZY samples. (b) Weight change and proton concentration as a function of temperature. Systematic errors are within the point size.

Table 2. Enthalpies and Entropies of Hydration Obtained by Thermogravimetric Studies

material	temperature range (°C)	P_{H_2O} (atm)	enthalpy (kJ mol^{-1})	entropy (J K^{-1} mol^{-1})	source
BZY10	100−500	0.019	−18 ± 2	−35 ± 3	this work
	500−900	0.019	−94 ± 12	−131 ± 13	this work
	500−800	0.005−0.04	−74 ± 3	−87 ± 10	29
	500−900	0.023	−79.4	−88.8	3
BZY20	200−500	0.019	−22 ± 4	−25 ± 6	this work
	50−500	0.023	−22 ± 1	−39 ± 1	6
	500−900	0.019	−98 ± 12	−122 ± 13	this work
	500−900	0.023	−93.9	−103.2	3
BZY30	300−500	0.019	−25 ± 6	−28 ± 9	this work
	50−500	0.023	−26 ± 1	−44 ± 1	6
	500−900	0.019	−141 ± 20	−166 ± 20	this work

energy barrier for proton migration into the sublayer. Based on DFT calculations, they also showed that the surface impedes proton conduction by 6 orders of magnitude compared to the bulk at 900 K.[31] Additionally, Jarry et al. showed for barium zirconate−barium cerate solid solutions that hydration is associated with surface secondary phase growth comprising oxygen-undercoordinated yttria and/or yttrium hydroxide,[32] which is in agreement with the space-charge compensation included in the defect model provided by Polfus et al.[5] Given the influence of the barium nonstoichiometry on the energetics of hydration shown by Yamazaki et al.,[21] such formation of secondary phases at higher relative pressures and higher proton concentration can explain the energetics of hydration at this region.

To fully analyze the phenomena occurring during hydration, all possible reactions should be taken into consideration. Another possible process apart from hydration is the water-based oxidation (7).

$$H_2O(g) + V_O^{\bullet\bullet} \rightarrow O_O^x + 2h^{\bullet} + H_2 \quad (7)$$

However, this reaction is less favorable than hydration, from a thermodynamic point of view, especially for low proton concentration.[33] For highly oxidizing conditions, the creation of electron holes due to oxidation is possible (8).

$$\frac{1}{2}O_2(g) + V_O^{\bullet\bullet} \rightarrow O_O^x + 2h^{\bullet} \quad (8)$$

In direct calorimetric measurements, the carrier gas being nitrogen ensured low oxygen partial pressure; therefore, the oxidation reaction can be neglected. Furthermore, the total proton concentration at a given temperature is the same for both thermogravimetric measurements held in high oxygen partial pressure and direct calorimetric measurements in nitrogen.

Apart from oxidation or reduction reactions, the formation of secondary phases (e.g., $BaCO_3$) would also be possible; however, the X-ray diffractograms (Figure 1) show no extra peaks for samples after hydration experiments. This suggests that the reaction between the sample and water vapor, visible in calorimetric data, should be associated with the water uptake reaction and not the formation of secondary phases. Moreover, the time scales of effects being observed in our experiments suggest that the observed phenomena are linked to water incorporation. The magnitudes of reaction enthalpies also indicate that the possible water splitting and chemical conversion are negligible. The magnitudes of enthalpies of water splitting are as high as 285 kJ/mol for the range up to 400 °C.[34,35]

https://dx.doi.org/10.1021/acs.jpcc.0c01049
J. Phys. Chem. C 2020, 124, 11308−11316

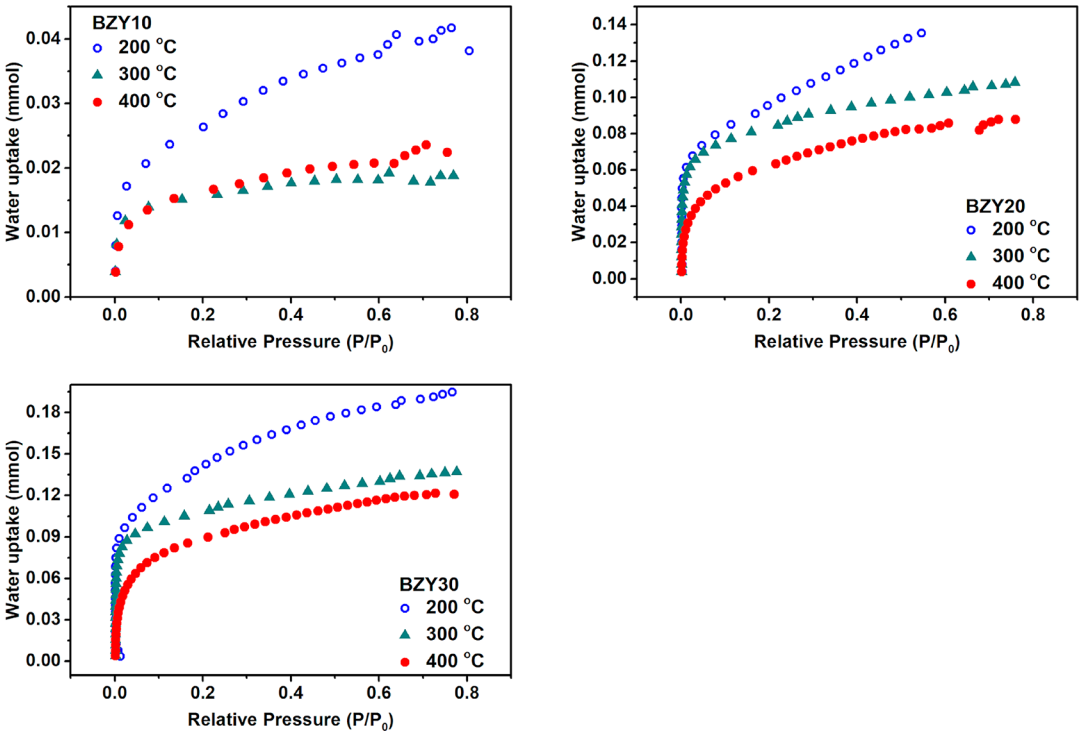

Figure 6. Water uptake of BZYx, x = 10, 20, and 30 mol %, as a function of relative water pressure (P/P_0) at different temperatures. Systematic errors are within the point size.

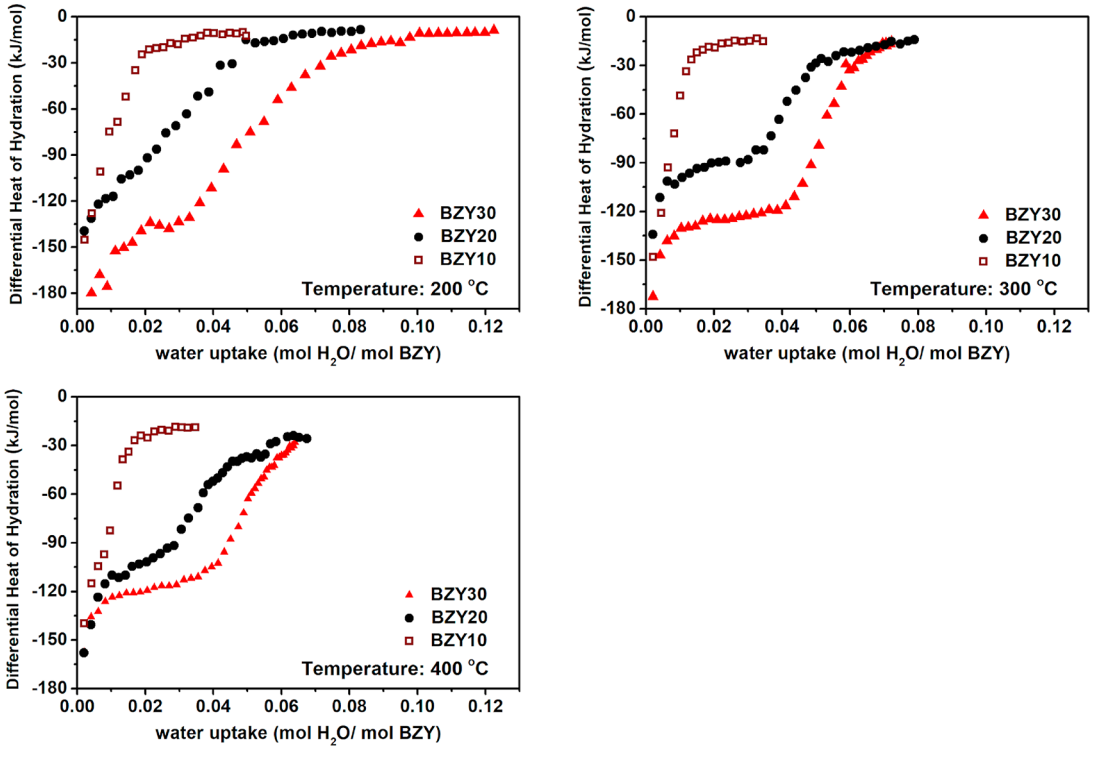

Figure 7. Differential enthalpy of hydration as a function of water uptake per mole of BZYx solid solutions, x = 10, 20, and 30 mol % of Y^{3+}, compared for each measurement temperature (200, 300, and 400 °C). Systematic errors are within the point size.

CONCLUSIONS

Water uptake studies on yttrium-doped barium zirconate, including variable yttrium content, 10−30 mol %, were conducted by two independent experimental methods, namely, thermogravimetry and direct isothermal water uptake calorimetry. For the first time, such an approach has been used for studying BZY systems. The water uptake and hydration energies determined using both methods for all studied compositions were comparable within and with the ones obtained in other studies. A three-step hydration process has been revealed by the

https://dx.doi.org/10.1021/acs.jpcc.0c01049
J. Phys. Chem. C 2020, 124, 11308−11316

Table 3. Total Water Uptake and Differential Enthalpy of Hydration (ΔH_{diff}) of BZYx, x = 10, 20, and 30 mol % of Y^{3+}, for the First and Last Dose Measured at Different Temperatures

sample	T (°C)	H_2O uptake (mol/mol of BZYx) (±0.001)	ΔH_{diff} (kJ/mol) (±1 kJ/mol) first dose	last dose
BZY10	200	0.023	−145	−10
	300	0.010	−148	−15
	400	0.013	−140	−19
BZY20	200	0.071	−140	−8
	300	0.057	−134	−14
	400	0.046	−158	−26
BZY30	200	0.103	−180	−9
	300	0.072	−172	−15
	400	0.064	−157	−30

hydration enthalpies, reflecting a balance between surface and bulk properties. The precise incremental water dosing along with the direct measurement of energetics with high resolution supports the dissociative incorporation of water in BZY, particularly at low proton concentration, as proposed by several other researchers based on overall hydration energies. These *in situ* hydration energetics show excellent benchmarking between traditional and direct microcalorimetric methods. We were able to reveal the stepwise process of protonation in barium zirconate protonation which shows the strong dependency of hydration thermodynamics and surface defect distribution. Moreover, by this study, we were also able to validate isobaric thermogravimetry as a suitable method for water uptake studies on proton conductors.

AUTHOR INFORMATION

Corresponding Author

Aleksandra Mielewczyk-Gryń − *Department of Solid State Physics, Faculty of Applied Physics and Mathematics, and Advanced Materials Centre, Gdańsk University of Technology, 80-233 Gdańsk, Poland;* orcid.org/0000-0001-6795-3840; Email: alegryn@pg.edu.pl

Authors

Mayra D. Gonçalves − *Peter A. Rock Thermochemistry Laboratory and NEAT ORU, University of California, Davis, Davis, California 95616, United States*

Pardha S. Maram − *Department of Chemistry, SRM University-AP, Neerukonda, Andhra Pradesh 522502, India;* orcid.org/0000-0002-1726-5086

Łukasz Kryścio − *Department of Solid State Physics, Faculty of Applied Physics and Mathematics, Gdańsk University of Technology, 80-233 Gdańsk, Poland*

Maria Gazda − *Department of Solid State Physics, Faculty of Applied Physics and Mathematics, Gdańsk University of Technology, 80-233 Gdańsk, Poland*

Alexandra Navrotsky − *School of Molecular Sciences and Center for Materials of the Universe, Arizona State University, Tempe, Arizona 85287, United States;* orcid.org/0000-0002-3260-0364

Complete contact information is available at: https://pubs.acs.org/10.1021/acs.jpcc.0c01049

Notes

The authors declare no competing financial interest.

ACKNOWLEDGMENTS

The thermochemical studies were supported by the U.S. Department of Energy, Office of Basic Energy Sciences, grant DE-FG02-03ER46053. A.M.-G., M.G., and Ł.K. acknowledge support from the Ministry of Science and Higher Education, Poland Grant No. IP2015 051374.

REFERENCES

(1) Kreuer, K.-D. Proton Conductivity: Materials and Applications. *Chem. Mater.* **1996**, *8* (3), 610−641.

(2) Bohn, H. G.; Schober, T. Electrical Conductivity of the High-Temperature Proton Conductor BaZr0.9Y0.1O2.95. *J. Am. Ceram. Soc.* **2000**, *83* (4), 768−772.

(3) Kreuer, K. D.; Adams, S.; Münch, W.; Fuchs, A.; Klock, U.; Maier, J. Proton Conducting Alkaline Earth Zirconates and Titanates for High Drain Electrochemical Applications. *Solid State Ionics* **2001**, *145* (1−4), 295−306.

(4) Giannici, F.; Shirpour, M.; Longo, A.; Martorana, A.; Merkle, R.; Maier, J. Long-Range and Short-Range Structure of Proton-Conducting Y:BaZrO $_3$. *Chem. Mater.* **2011**, *23* (11), 2994−3002.

(5) Polfus, J. M.; Bjørheim, T. S.; Norby, T.; Bredesen, R. Surface Defect Chemistry of Y-Substituted and Hydrated $BaZrO_3$ with Subsurface Space-Charge Regions. *J. Mater. Chem. A* **2016**, *4* (19), 7437−7444.

(6) Yamazaki, Y.; Babilo, P.; Haile, S. M. Defect Chemistry of Yttrium-Doped Barium Zirconate: A Thermodynamic Analysis of Water Uptake. *Chem. Mater.* **2008**, *20* (20), 6352−6357.

(7) Kreuer, K. D. Aspects of the Formation and Mobility of Protonic Charge Carriers and the Stability of Perovskite-Type Oxides. *Solid State Ionics* **1999**, *125* (1-4), 285−302.

(8) Chang, C.-H.; Gong, M.; Dey, S.; Liu, F.; Castro, R. H. R. Thermodynamic Stability of SnO $_2$ Nanoparticles: The Role of Interface Energies and Dopants. *J. Phys. Chem. C* **2015**, *119* (11), 6389−6397.

(9) Castro, R. H. R.; Quach, D. V. Analysis of Anhydrous and Hydrated Surface Energies of Gamma-Al $_2$ O $_3$ by Water Adsorption Microcalorimetry. *J. Phys. Chem. C* **2012**, *116* (46), 24726−24733.

(10) Ushakov, S. V.; Navrotsky, A. Direct Measurements of Water Adsorption Enthalpy on Hafnia and Zirconia. *Appl. Phys. Lett.* **2005**, *87* (16), 164103.

(11) Norby, T.; Widerøe, M.; Glöckner, R.; Larring, Y. Hydrogen in Oxides. *Dalt. Trans.* **2004**, 3012−3018.

(12) Tsvetkov, D. S.; Maram, P. S.; Tsvetkova, N. S.; Zuev, A. Y.; Navrotsky, A. High-Resolution Thermochemical Study of Phase Stability and Rapid Oxygen Incorporation in YBaCo 4- x Zn x O 7+δ 114-Cobaltites. *J. Phys. Chem. A* **2018**, *122* (50), 9597−9604.

(13) Costa, G. C. C.; Saradhi Maram, P.; Navrotsky, A. Thermodynamics of Nanoscale Lead Titanate and Barium Titanate Perovskites. *J. Am. Ceram. Soc.* **2012**, *95* (10), 3254−3262.

(14) Drazin, J. W.; Castro, R. H. R. Water Adsorption Microcalorimetry Model: Deciphering Surface Energies and Water Chemical Potentials of Nanocrystalline Oxides. *J. Phys. Chem. C* **2014**, *118* (19), 10131−10142.

(15) Boschini, F.; Robertz, B.; Rulmont, A.; Cloots, R. Preparation of Nanosized Barium Zirconate Powder by Thermal Decomposition of Urea in an Aqueous Solution Containing Barium and Zirconium, and by Calcination of the Precipitate. *J. Eur. Ceram. Soc.* **2003**, *23* (16), 3035−3042.

(16) Nuñez, G.; Balanay, M. J.; Cervera, R. B. M. Preparation of Y-Doped $BaZrO_3$; Proton Conducting Solid Electrolyte via Modified Low Temperature Pechini Method. *Adv. Mater. Res.* **2015**, *1098*, 86−91.

(17) Zagórski, K.; Wachowski, S.; Szymczewska, D.; Mielewczyk-Gryń, A.; Jasiński, P.; Gazda, M. Performance of a Single Layer Fuel Cell Based on a Mixed Proton-Electron Conducting Composite. *J. Power Sources* **2017**, *353*, 230−236.

(18) Fabbri, E.; Pergolesi, D.; Traversa, E. Materials Challenges toward Proton-Conducting Oxide Fuel Cells: A Critical Review. *Chem. Soc. Rev.* **2010**, *39* (11), 4355.
(19) Sažinas, R.; Einarsrud, M.-A.; Grande, T. Toughening of Y-Doped $BaZrO_3$ Proton Conducting Electrolytes by Hydration. *J. Mater. Chem. A* **2017**, *5* (12), 5846−5857.
(20) Kreuer, K. D. Proton-Conducting Oxides. *Annu. Rev. Mater. Res.* **2003**, *33* (1), 333−359.
(21) Yamazaki, Y.; Yang, C.-K. K.; Haile, S. M. *Scr. Mater.* **2011**, *65*, 102−107.
(22) Gonçalves, M. D.; Maram, P. S.; Muccillo, R.; Navrotsky, A. Enthalpy of Formation and Thermodynamic Insights into Yttrium Doped BaZrO 3. *J. Mater. Chem. A* **2014**, *2* (42), 17840−17847.
(23) Yamazaki, Y.; Blanc, F.; Okuyama, Y.; Buannic, L.; Lucio-Vega, J. C.; Grey, C. P.; Haile, S. M. Proton Trapping in Yttrium-Doped Barium Zirconate. *Nat. Mater.* **2013**, *12* (7), 647−651.
(24) Yamazaki, Y.; Hernandez-Sanchez, R.; Haile, S. M. Cation Non-Stoichiometry in Yttrium-Doped Barium Zirconate: Phase Behavior, Microstructure, and Proton Conductivity. *J. Mater. Chem.* **2010**, *20* (37), 8158.
(25) Nomura, K.; Kageyama, H. Transport Properties of Ba-(Zr0.8Y0.2)O3 − δ Perovskite. *Solid State Ionics* **2007**, *178* (7−10), 661−665.
(26) Gonçalves, M. D.; Maram, P. S.; Navrotsky, A.; Muccillo, R. Effect of Synthesis Atmosphere on the Proton Conductivity of Y-Doped Barium Zirconate Solid Electrolytes. *Ceram. Int.* **2016**, *42* (12), 13689−13696.
(27) Takahashi, H.; Yashima, I.; Amezawa, K.; Eguchi, K.; Matsumoto, H.; Takamura, H.; Yamaguchi, S. First-Principles Calculations for the Energetics of the Hydration Reaction of Acceptor-Doped $BaZrO_3$. *Chem. Mater.* **2017**, *29* (4), 1518−1526.
(28) Putilov, L. P.; Tsidilkovski, V. I. Impact of Bound Ionic Defects on the Hydration of Acceptor-Doped Proton-Conducting Perovskites. *Phys. Chem. Chem. Phys.* **2019**, *21* (12), 6391−6406.
(29) Schober, T.; Bohn, H. G. Water Vapor Solubility and Electrochemical Characterization of the High Temperature Proton Conductor BaZr0.9Y0.1O2.95. *Solid State Ionics* **2000**, *127* (3), 351−360.
(30) Polfus, J. M.; Yang, J.; Yildiz, B. *J. Mater. Chem. A* **2018**, *6*, 24823.
(31) Kim, J.-S.; Kim, Y.-C. Proton Conduction across and along BaO− and ZrO2−Terminated (001) BaZrO3 Surfaces Using Density Functional Theory. *Solid State Ionics* **2017**, *306*, 137−141.
(32) Jarry, A.; Ricote, S.; Geller, A.; Pellegrinelli, C.; Zhang, X.; Stewart, D.; Takeuchi, I.; Wachsman, E.; Crumlin, E. J.; Eichhorn, B. Assessing Substitution Effects on Surface Chemistry by in Situ Ambient Pressure X-Ray Photoelectron Spectroscopy on Perovskite Thin Films, $BaCe_x Zr_{0.9-x} Y_{0.1} O_{2.95}$ (x = 0; 0.2; 0.9). *ACS Appl. Mater. Interfaces* **2018**, *10* (43), 37661−37670.
(33) Benediktsson, M. T. A Theoretical Study of Doping and the Hydration Process of Barium Zirconate; Chalmers University of Technology, 2013.
(34) Nong, G.; Li, Y.; Yin, Y. Energy Analysis on the Water Cycle Consisting of Photo Catalyzing Water Splitting and Hydrogen Reacting with Oxygen in a Hydrogen Fuel Cell. *Chem. Phys. Lett. X* **2019**, *4*, 100033.
(35) Smolinka, T. Fuels - Hydrogen Production | Water Electrolysis. In *Encyclopedia of Electrochemical Power Sources*; Elsevier: 2009; pp 394−413. DOI: 10.1016/B978-044452745-5.00315-4.

https://dx.doi.org/10.1021/acs.jpcc.0c01049
J. Phys. Chem. C 2020, 124, 11308−11316